



OPEN

Surface ocean microbiota determine cloud precursors

Karine Sellegri¹✉, Alessia Nicosia¹, Evelyn Freney¹, Julia Uitz², Melilotus Thyssen³, Gérald Grégori³, Anja Engel⁴, Birthe Zäncker⁴, Nils Haëntjens⁵, Sébastien Mas⁶, David Picard¹, Alexia Saint-Macary^{7,8}, Maija Peltola¹, Clémence Rose¹, Jonathan Trueblood¹, Dominique Lefevre³, Barbara D'Anna⁹, Karine Desboeufs¹⁰, Nicholas Meskhidze¹¹, Cécile Guieu² & Cliff S. Law^{7,8}

One pathway by which the oceans influence climate is via the emission of sea spray that may subsequently influence cloud properties. Sea spray emissions are known to be dependent on atmospheric and oceanic physicochemical parameters, but the potential role of ocean biology on sea spray fluxes remains poorly characterized. Here we show a consistent significant relationship between seawater nanophytoplankton cell abundances and sea-spray derived Cloud Condensation Nuclei (CCN) number fluxes, generated using water from three different oceanic regions. This sensitivity of CCN number fluxes to ocean biology is currently unaccounted for in climate models yet our measurements indicate that it influences fluxes by more than one order of magnitude over the range of phytoplankton investigated.

The natural variability of sea spray aerosol (SSA) number fluxes and chemical composition is poorly understood, yet it has been shown to play a major role in the Earth climate system¹, largely through their effect on maritime cloud properties. Cloud radiative properties depend on cloud droplet number concentrations (CDNC)^{2,3}, which are a function of atmospheric particle concentrations that serve as cloud condensation nuclei (CCN). In the Southern Ocean, a region with limited anthropogenic aerosols, SSA may contribute a significant fraction of the CCN⁴ leading to elevated CDNCs in low-level maritime boundary layer clouds⁵. Despite elevated CDNCs in the Southern Ocean being associated with regions of high Chlorophyll-a (Chl-a) concentration^{6,7}, the processes linking marine biota, marine aerosols, and CDNC are still not well understood and remain a topic of a three-decades long debate⁸. Although the biogenic origin of organic matter in sea spray has been extensively studied^{9–13}, empirical evidence that marine biota modifies the sea spray number concentration flux to the atmosphere is scarce¹⁴ and yet to be formalized. Laboratory studies have shown an increase of SSA number concentrations related to organic exudates, phytoplankton and/or bacteria^{15,16} and some in-situ studies have suggested that SSA number concentration and organic content are related^{17–19}. An elevated sea spray number production was observed for SSA generated from biologically productive seawaters relative to oligotrophic waters^{15–20}. However, to our knowledge, a quantitative link between phytoplankton groups and SSA number fluxes, a critical component for simulating the impact of marine aerosols on CCN number concentrations²¹ and climate²², has not been established.

Relevant sea spray emission properties for cloud condensation nuclei fluxes. CCN number fluxes measured from a continuous flow-through underway seawater plunging jet system¹³ varied by a factor of 3 along the ship track in the Mediterranean Sea (Fig. 1c). The variability of the CCN concentration may depend on the variability in the available SSA hygroscopicity, size, and number concentration, each of which was tested. According to Fig. 1a, the activation diameter of sea spray at 0.1% supersaturation is stable at ~100 nm, indicat-

¹Laboratoire de Météorologie Physique (LaMP), Université Clermont Auvergne, CNRS, 63000 Clermont-Ferrand, France. ²Laboratoire d'Océanographie de Villefranche (LOV), Sorbonne Université, CNRS, 06230 Villefranche-sur-Mer, France. ³Mediterranean Institute of Oceanography UM110, Aix-Marseille University, Toulon University, CNRS, IRD, 13288 Marseille, France. ⁴GEOMAR, Helmholtz Centre for Ocean Research, 24105 Kiel, Germany. ⁵School of Marine Sciences, University of Maine, Orono, ME 04469, USA. ⁶MEDIMEER, UMS3282 OSU OREME, Université de Montpellier, CNRS, IRD, Sète, France. ⁷National Institute of Water and Atmospheric Research (NIWA), Wellington, New Zealand. ⁸Department of Marine Sciences, University of Otago, Dunedin, New Zealand. ⁹Laboratoire Chimie Environnement (LCE), UMR 7673 CNRS, Université Aix-Marseille, 13331 Marseille, France. ¹⁰LISA, UMR CNRS 7583, Institut Pierre Simon Laplace (IPSL), Université de Paris, Université Paris-Est-Créteil, Créteil, France. ¹¹North Carolina State University, Raleigh, USA. ✉email: K.Sellegri@opgc.cnrs.fr

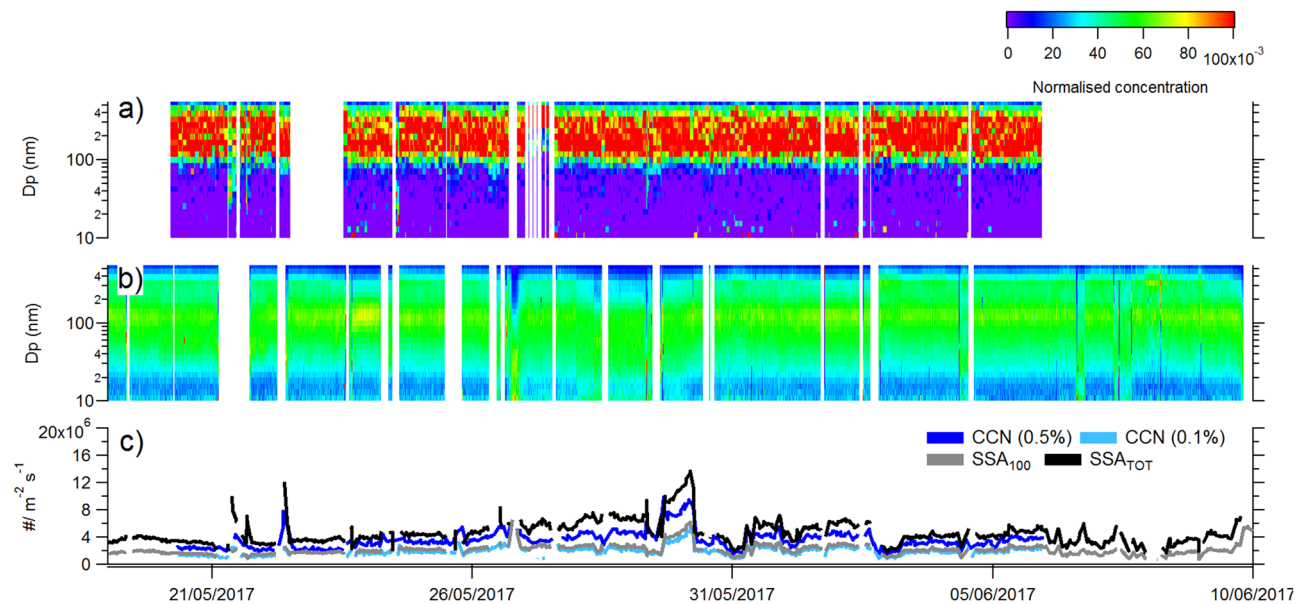


Figure 1. Time series along the PEACETIME (ProcEss studies at the Air-sEa Interface after dust deposition in The Mediterranean sea) ship track of (a) $CCN_{0.1\%}$ concentrations normalized to the sea spray concentration at given particle diameter (D_p). The activation diameter of SSA into cloud droplet at 0.1% supersaturation is visible at the change of colour from purple to red (b) sea spray concentration at given diameters (D_p) normalized with the total sea spray concentration, (c) flux of sea spray aerosol number (SSA_{TOT}), flux of sea spray larger than 100 nm number (SSA_{100}), and flux of CCN at 0.5% and 0.1% supersaturation, $CCN_{0.5\%}$ and $CCN_{0.1\%}$, respectively.

ing very little changes in hygroscopicity of SSA. Hence, changes in the hygroscopic properties of SSA alone were insufficient to explain the observed spatial and temporal variation of the CCN number fluxes over different regions of the Mediterranean Sea. The average size distribution of SSA was dominated by 115 nm particles (see lognormal mode characteristics in the Supplementary Information (SI)) and showed little variation along the ship's track as well (Fig. 1b), consistent with previous experiments in the Mediterranean Sea^{13,23}. This indicates that changes in the size of SSA were not able to explain the variation in CCN production fluxes neither. It can be seen in Fig. 1c that the variations in the CCN number fluxes closely follow the variations in the SSA number flux. The cloud condensation nuclei flux at 0.1% supersaturation ($CCN_{0.1\%}$ flux) can be predicted with a mean 13% accuracy from the number flux of sea spray particles greater than 100 nm (SSA_{100} flux) ($CCN_{0.1\%} = 0.78 * SSA_{100} + 72$; $R = 0.88$), independently of the SSA size and hygroscopicity. As there are more data available for SSA number fluxes than CCN number fluxes, we will in the following discussion focus on the environmental factors influencing the SSA_{100} flux, assumed to control the $CCN_{0.1\%}$ flux to the atmosphere.

Seawater properties determine sea spray number fluxes. CCN number and CDNC have only been tentatively, but not consistently, related to seawater Chl-*a* concentration in the literature, indicating that Chl-*a* is not an optimal proxy for predicting marine CCN fluxes. In the Mediterranean Sea, the Chl-*a* spatial variation did not match the sea spray originating CCN spatial variation (Fig. S2a,b). Amongst the other seawater biological parameters measured (including nanoeukaryotes, picoeukaryotes, coccolithophores, cryptophytes and *Synechococcus* cell abundances), the strongest linear correlation was observed between SSA_{100} and nanoeukaryotic cell abundance (NanoPhyto) ($R = 0.39$, $p < 0.001$) (Fig. 2). We further examined the relationship between SSA_{100} and the nanophytoplankton cell abundance in other data sets.

Similar SSA generation experiments were performed using South West Pacific (NZ coastal) and Arctic coastal waters at different periods of the year. The NZ coastal waters were sampled during the austral spring when productivity was elevated. When relating the SSA_{100} production flux (F_{CN100}) from the NZ coastal waters to biogeochemical seawater properties, the highest correlations were again observed with NanoPhyto cell abundances, with similar coefficients to that of Mediterranean oligotrophic waters (Table 1). To account for the temperature dependence of SSA number production fluxes^{26,27} in the different data sets, all fluxes were normalized to a 15 °C SST, following Salter et al. (2015). The merged data sets provided a single linear relationship between F_{SSA100} and NanoPhyto (Fig. 3) with a greater statistical significance (higher R value) than the individual regional data sets (Table 1). Using the resulting linear relationship between F_{SSA100} and NanoPhyto for the merged data set, we define the F_{SSA100} in biologically-free seawaters, i.e. containing only inorganic chemical components ($F_{SSA100INORG}$) as the intercept of the y axis ($2.1 \times 10^5 \text{ m}^{-2} \text{ s}^{-1}$). We then express F_{SSA100} as a function of $F_{SSA100INORG}$ in Eq. (1) for a larger use of our parameterization in regional and global models.

$$F_{SSA100} = (1.18 \times 10^{-2} * \text{NanoPhyto} + 1) * F_{SSA100INORG} \quad (1)$$

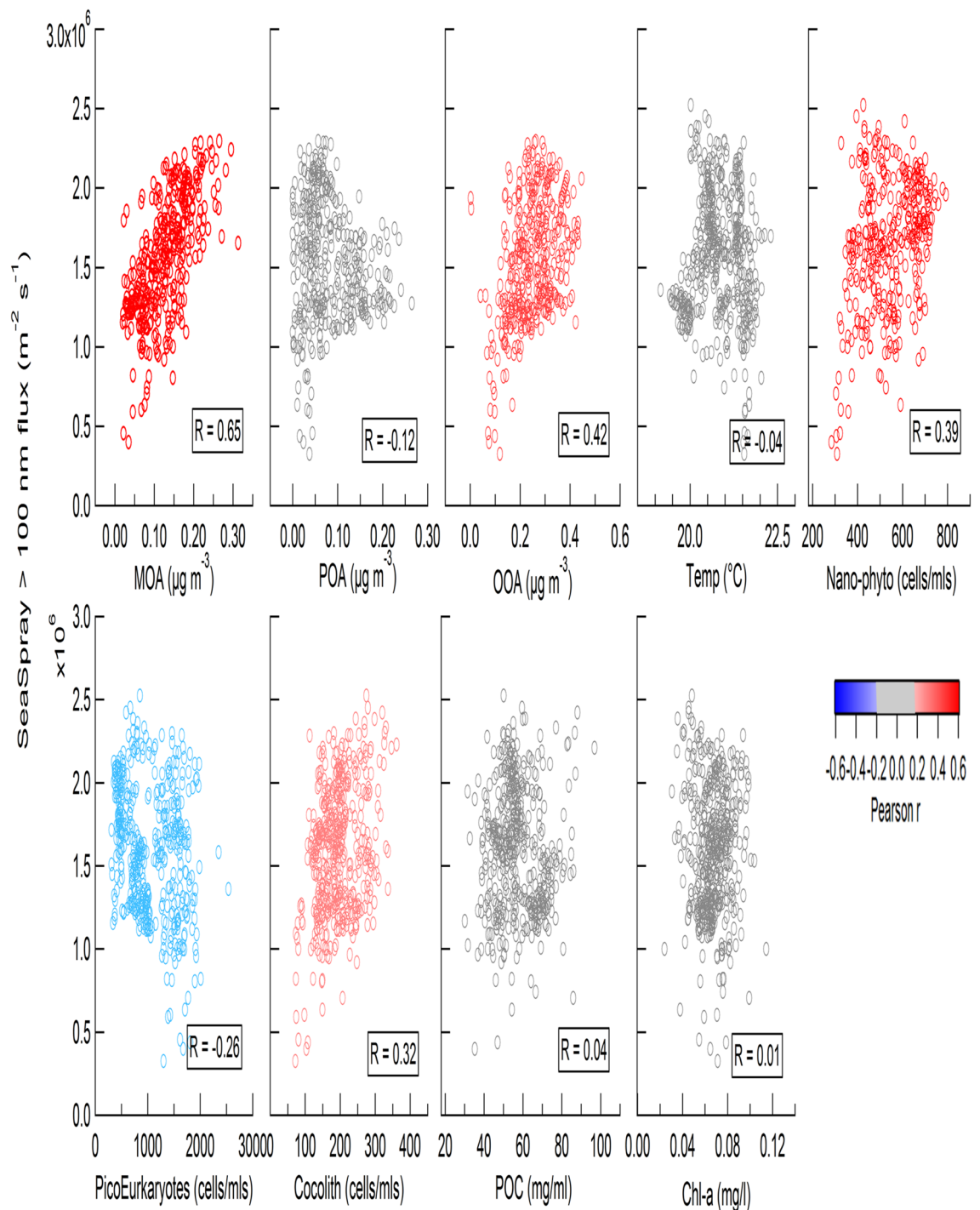


Figure 2. Correlation plots between the sea spray larger than 100 nm number fluxes ($\text{m}^{-2} \text{cm}^{-1}$) and the three classes of organic matter in nascent sea spray (MOA, POA, OOA), Sea Surface Temperature (SST, $^{\circ}\text{C}$), seawater cell abundances (cells ml^{-1}) for nanoeukaryotes (2–20 μm size; *NanoPhyto*), picoplankton (3 μm or less in size), coccolithophore-like cells, particulate organic carbon (POC, mg ml^{-1}), and total surface Chl-*a* ($\mu\text{g l}^{-1}$), from the Mediterranean cruise data set. Red datapoints indicate a significant positive correlation, Blue a significant negative correlation and grey no significant relationship at the 99.9% confidence level.

Although the NZ coastal data set shows a large *NanoPhyto* range and the F_{SSA100} –*NanoPhyto* relationship is similar to that of the Mediterranean dataset, combining all data sets provides the broadest coverage of F_{SSA100} and *NanoPhyto*. Therefore, we suggest that this correlation, derived from a two-orders of magnitude range of *NanoPhyto* cell abundances, could, as a first approximation, be applicable to the spatial range and trophic diversity across the global oceans. However, while *NanoPhyto* were almost absent in Arctic seawater during

Seawater geographical origin	a	b	R	Rho	P value	Chl-a ($\mu\text{g l}^{-1}$)	NanoPhyto (cells ml^{-1})
Mediterranean	2.17×10^3	3.83×10^5	0.72	0.51	<.00001	0.03 ± 0.01 0.02–0.04	546 ± 148 390–703
South west Pacific	2.20×10^3	2.04×10^6	0.77	0.85	<.00001	2.13 ± 0.40 1.65–2.60	4880 ± 2390 1840–8250
Arctic	–	–	–	–	–	0.01–0.3	4.2 ± 4.3 0–9.4
Merged Mediterranean, NZ coastal and Arctic	2.48×10^3	2.10×10^5	0.90	0.60	<.00001	0.01–2.60	0–8250

Table 1. Fitting parameters (a and b) and correlation coefficients (Pearson R) for the linear relationship between the production flux of SSA100 (F_{SSA100} , $\text{m}^{-2} \text{s}^{-1}$) and eukaryotic nanophytoplankton cell abundance (NanoPhyto, in cells ml^{-1}) in the form of $F_{\text{SSA100}} = a * \text{NanoPhyto} + b$ for a wind speed of 9 m s^{-1} and temperature of $15 \text{ }^\circ\text{C}$. The correlation coefficient Spearman Rho between these two variables is also indicated. Average, standard deviation and range (10–90 percentiles) of Chl-a and NanoPhyto for the three measurement campaigns.

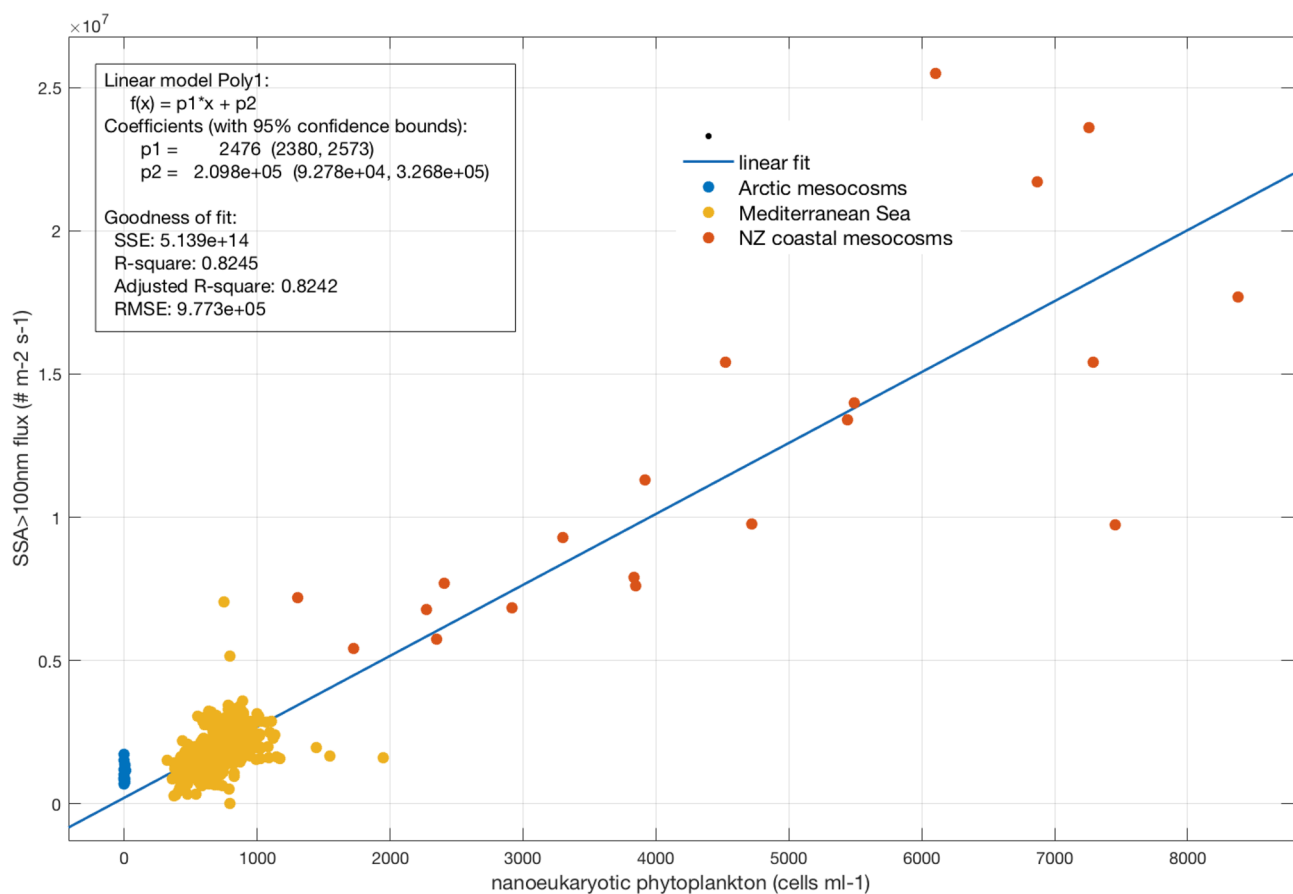


Figure 3. SSA larger than 100 nm flux number F_{SSA100} ($\# \text{ m}^{-2} \text{ s}^{-1}$) calculated for a wind speed of 9 m s^{-1} and $15 \text{ }^\circ\text{C}$ sea temperature as a function of the NanoPhyto (cells ml^{-1}) from different regions. The solid line indicates the linear fit to the data set.

early springtime (Table 1), the average F_{SSA100} obtained for this data set ($1.1 \times 10^6 \text{ m}^{-2} \text{ s}^{-1}$), although close to $F_{\text{SSA100INORG}}$, still differs by a factor of 5. This lack of agreement suggests that a different parameter is controlling F_{SSA100} in the Arctic mesocosm experiment. This illustrates the need for a better mechanistic understanding of the factors driving the relationship between NanoPhyto and F_{SSA100} .

Potential mechanisms for a biologically driven sea spray number fluxes. We examined relationships between SSA_{100} and organic content of SSA. In the Mediterranean dataset, three main groups of organic species with different oxidation levels were identified in SSA using a positive matrix factorization: a primary-like OA group (POA), an oxidized organic group (OOA), and a mixed (primary and oxidized) group (MOA)²⁵. As shown in Fig. 2, SSA_{100} showed the strongest correlation with MOA ($R=0.65$, $p<0.001$) with a higher signifi-

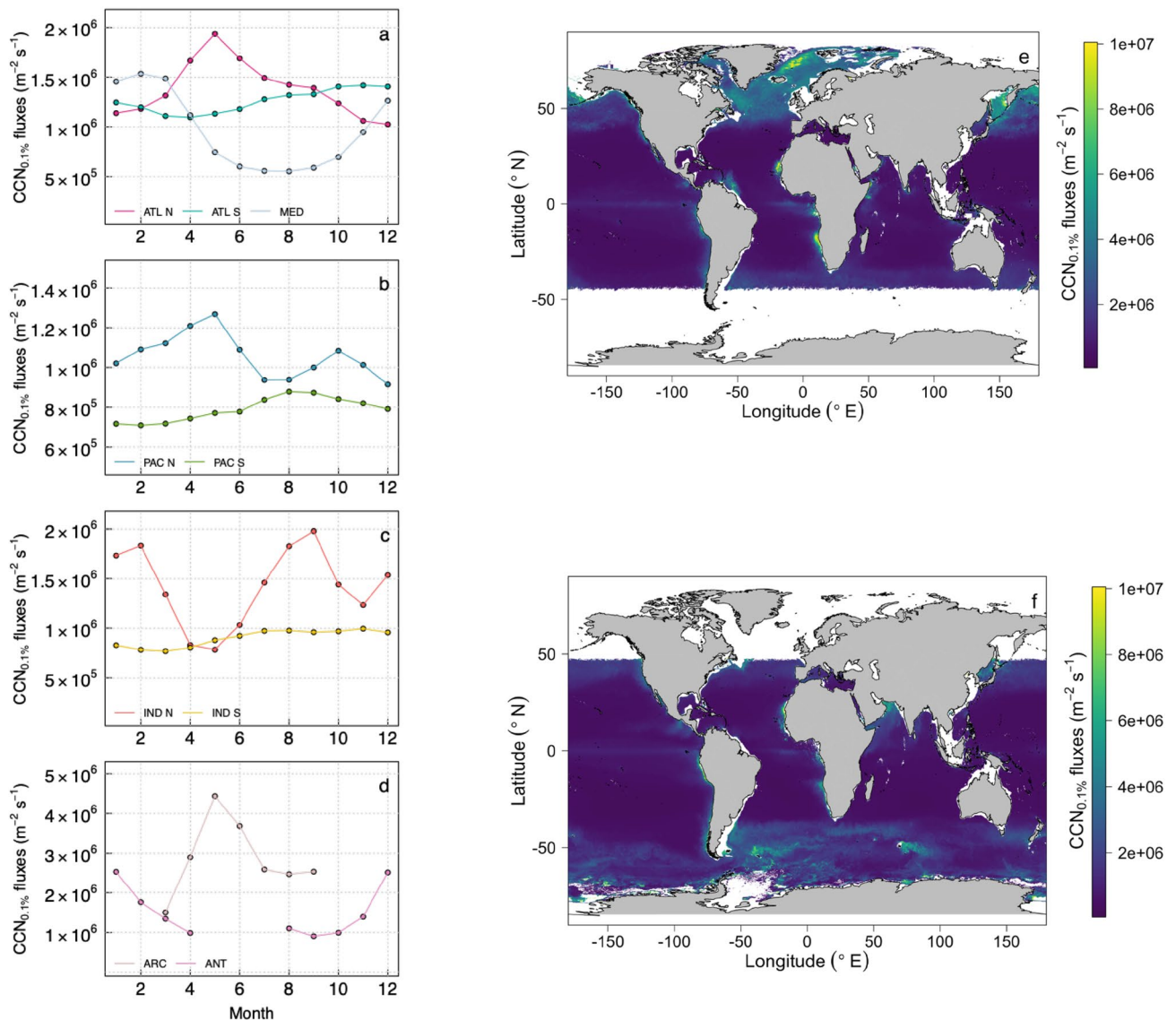


Figure 4. Global CCN_{0.1%} emission fluxes (m⁻² s⁻¹) computed for a 15 °C temperature from satellite-based nanoplankton cell abundance in June (e) and December (f). CCN fluxes were computed using Eq. (1), and assuming that CCN_{0.1%} is equal to SSA₁₀₀. Median annual trends are represented for the different oceanic basins (a) ATL N: North Atlantic, ATL S: South Atlantic, MED: Mediterranean Sea; (b) PAC N: North Pacific, PAC S (South Pacific), (c) IND N (North Indian Ocean), IND S (South Indian Ocean), (d) ARC (Arctic Ocean), ANT (Southern Ocean). Maps provided (e,f) were created using R version 3.4.2. (<https://www.R-project.org/>).

cance than for the correlation between NanoPhyto and SSA₁₀₀ ($R=0.39$, $p<0.001$); this infers that NanoPhyto influence SSA₁₀₀ by producing MOA but may not be the only source of MOA. The organic mass fraction of sub-micron nascent sea spray did not vary significantly along the cruise track ($22 \pm 6\%$) and the contribution of MOA to total sea spray mass is less than 2%. Therefore, the hypothesis that organics simply added to the inorganic sea salt flux cannot explain the observed F_{SSA100} increase by a factor 3 with MOA.

The most plausible mechanism is that F_{SSA100} is influenced by the presence of organics surfactants in the seawater and surface microlayer (SML)²⁸ which influence bubble bursting. This hypothesis is based on the fact that the SML is considered to be formed very rapidly (on the order of less than 20 s) via bubbling²⁹, and hence a SML would have been present in the sea spray generator. Organic surfactants may have different effects on the stability of bubbles. Soluble surfactants lead to higher bubble lifetimes (foam stabilization effect), making bubbles films thinner and hence decreasing the SSA number fluxes to the atmosphere^{30,31}. On the contrary, the presence of fatty acids suppresses foam formation, leading to shorter bubble lifetimes and hence thicker bubble films with the effect of increasing SSA number fluxes^{32,33}. MOA concentrations measured in the Mediterranean SSA were correlated with the enrichment of DOC in the SML relative to the underlying surface seawater²⁸, suggesting that MOA is itself enriched in the SML due to surface active properties. The MOA mass spectrum in the Mediterranean SSA contained mixed signatures of amino acids and fatty acids that were potentially responsible for the observed decrease in surface tension²⁵. In the NZ coastal seawater, surface tension decreased with

increasing seawater particulate saturated fatty acid concentration ($R=0.66$, $p<0.01$). In the Mediterranean data set, we also found that SSA_{100} is correlated with Transparent Exopolymer Particles (TEP) abundance ($R=0.46$, $p<0.01$), which are microgels that are produced by coagulation of phytoplankton exudates and also have surface active properties³⁴. The correlations between SSA and the different organic tracers measured during the different campaigns point to the presence of fatty acids combined with other organics, originating from exudates, in shaping the sea spray fluxes. In line with this hypothesis, past studies have shown a synergistic effect of surfactant mixtures on SSA fluxes compared to single component monolayers³³ and lipopolycarbonates were found to be a major fraction of marine primary organic matter³⁵. Particulate fatty acids are the main components of lipids in cell membranes, therefore they are of primary origin, and the lack of a clear diurnal variation of SSA_{100} (Fig. S2a), suggests that the SSA flux variability is not a result of aqueous-phase photochemistry. The absence of a temporal shift between high NanoPhyto and high F_{SSA} indicates that if organics are released by cell lysis, as suggested by earlier studies^{12,36,37} the process is continuous.

We have made a step towards a mechanistic understanding of the processes responsible for the increase of the SSA number fluxes using seawater biology, and we propose that this mechanism is primarily the influence of organic matter on bubble lifetime; however, more work is required to further ascertain this hypothesis. The relationship between nanoeukaryotes and MOA, and particularly whether certain species are responsible for the release of surface active compounds, requires further research. In the NZ coastal mesocosms, the small pennate diatom species *Nitzschia closterium* represented a significant fraction of the nanophytoplankton, and was also significantly correlated to SSA_{100} number concentration ($R=0.70$, $p<0.001$), but we do not have species information for the NanoPhyto in the other two datasets. However, establishing these relationships in natural marine systems is a first step towards identification of the mechanistic processes that will stimulate further research.

Impact on the variability of CCN fluxes driven by the marine biota and future implications. The variability of $CCN_{0.1\%}$ number fluxes at the global scale resulting from the spatial and temporal variations of NanoPhyto was computed using the ocean colour satellite-based phytoplankton group retrieval following Uitz et al.³⁸ and the parameterization given Eq. (1), with the assumption that all SSA_{100} will activate at 0.1% supersaturation. During summer, the resulting $CCN_{0.1\%}$ number fluxes are a factor of 5 higher at high latitudes compared to the subtropical areas in a given hemisphere (Fig. 4). Fluxes show little seasonal variation in the subtropical and tropical zones but can vary by at least a factor of 2 between winter and summer at high latitudes (Fig. 4). Currently, the impact of surface ocean biogeochemistry is only considered in global models by the addition of simulated marine organic matter to the CCN mass, which is predicted to increase CCN number concentration by <50%³⁹. From our results, the biological impact on the CCN flux number via its role in the bubble bursting process may be much higher (by up to a factor 5) than this 50% increase.

Methods

Field campaigns description. In the frame of the PEACETIME (MERMEX CHARMEX) project, an oceanographic cruise (<https://doi.org/10.17600/17000300>) onboard the R/V 'Pourquoi Pas?' took place in the Western/Central Mediterranean Sea May 10–June 11, 2017. The Mediterranean Sea was typical of oligotrophic conditions throughout the transect characterized by shallow mixed layer depth, low nutrients and chlorophyll-a concentrations. A clean pumping system enabled continuous sampling of seawater at 5 m depth and transfer to a sea spray generation device. In parallel, a number of parameters characterized surface water during the whole transect (2800 nautical miles).

The ME3 campaign was organized in New Zealand coastal waters (Evans Bay) in November 2017. The experimental setup consisted of three mesocosms containing 4200 l of seawater and 170 l headspace flushed with filtered air. Nutrients were added to all mesocosms daily over 21 days. One mesocosm served as control while one mimicked conditions of year 2100 (temperature increased by 2.6 °C and pH lowered by 0.5) and one mimicked conditions of year 2150 (temperature increased by 4.5 °C and pH lowered by 0.33). A total of 3.4 L of water collected from each mesocosm at 2 m depth from a well-mixed water column was used daily to generate sea spray as described below.

The Arctic mesocosm experiment was carried out in the framework of the MACA project (Marine Aerosol impact on Clouds in the Arctic) from the 5th to the 22nd of March 2017 in the Kongsfjorden next to the Ny-Alesund research station (78°55'42.5" N 11°56'13.3" E), Svalbard. The goal of the MACA project was to evaluate the impact of pollution on marine aerosol emission and cloud-related properties. Mesocosms enclosed 2260 L of seawater and 1 m³ of natural particle filtered air in a UV-transparent enclosure. Three mesocosms were used, one as a control, and the two others seeded with ammonium sulfate and ammonium nitrate rich rainwater, at concentrations typical of an average rain occurring in the area, and three times this average rain water concentration. Mesocosms were sampled daily from the 5th of March to the 22nd of March, with the exception during the 10th and the 11th due to bad weather conditions. Collection of samples were performed in the early morning using 20 L polycarbonate carboys, cleaned with ultrapure water at 1 m depth in well mixed water columns. A total of 3.4 L of water collected from each mesocosm was used daily to generate sea spray as described below.

Nascent sea spray generation and characterization. The same sea spray generation device was used in all three campaigns (PEACETIME, ME3, MACA), and was previously described in Schwier et al. (2015, 2017)^{13,24}. Experimental procedures used to generate nascent sea spray particles were also similar in all experiments, with the exception that the sea spray in the Mediterranean was generated continuously, while the sea sprays from NZ-coastal and Arctic mesocosms were generated as discrete daily samples. Briefly, the sea spray generator consists of a glass tank—20 × 20 cm and 25 cm high— which is filled with 3.6 L of seawater. In the remaining volume, particle-free air is flushed to maintain a constant over-pressure. The air flush, which was

kept constant over the course of each measurement campaign, was similar for all three experiments (Mediterranean, Arctic, NZ coastal) and served to reproduce the wind and ensure the absence of ambient room particles. Inside the sea spray generator, seawater was forced through eight 1 mm nozzles and form vertical plunging jets. The plunging jet creates an air entrainment that reproduces the bubble size distribution naturally equivalent to the bubble size distribution of natural wave breaking^{40,41}. The water flow rate ranged from 1.6 to 1.8 L min⁻¹ depending on the experiment but was kept constant throughout each experiment. During PEACETIME, the system was used with seawater circulating in an open loop, continuously circulating under way seawater with a peristaltic pump. This type of sea spray generator was shown to successfully reproduce the average size distribution shape of ambient aerosols sampled in clean oceanic sector^{40,41}. Upscaling of the fluxes obtained using the plunging jets system to ambient wind dependent SSA fluxes is described in the production flux calculation section. The temperature of the seawater present in the sea spray generator varied according to the experiment. For the PEACETIME dataset, SST followed the underway SST and stayed fairly constant at 20.4 ± 1.2 °C. For the Arctic and NZ coastal water experiments, SSW temperature during sea spray generation were 13.4 ± 1.9 °C and 17.7 ± 2.2 °C respectively.

A CCNc-DMPS instrument was connected to the sea spray generator for measuring the sea spray number size distribution, and CCN number size distribution simultaneously. The custom-made instrument consists of a 2.5 micron impactor preventing large sea spray from entering the instrument, an aerosol neutralizer, a differential mobility Analyzer (DMA) column to select sea spray per size, followed by a Condensation Particle Counter (CPC) and a miniature continuous-flow stream-wise thermal-gradient CCN chamber (CCNc) in parallel. A CPC TSI 3010 was used in parallel to the DMPS, for quality check of the DMPS size distributions. All aerosol properties were measured after the aerosol was dried through a 1 m diffusion dryer after the sea spray generator, leading to < 40% RH in the instruments. Activation diameters at which sea spray activates to cloud droplets were calculated as described in Asmi et al. (2012)⁴². The chemical composition of sea spray was obtained using a Time of Flight Aerosol Chemical Speciation Monitor (ToF-ACSM⁴³), on-line from the sea spray generator for the PEACETIME campaign. The treatment of data from the ACSM instrument and the subsequent positive matrix factorization of the measured organic aerosol²⁵. A brief description will be provided here. Data acquired with the ToF-ACSM was analysed using ToFWARE v2.6.11. Raw aerosol mass spectra were treated with a modified version of the standard fragmentation table⁴⁴. Since the ACSM instrument was sampling seawater directly the contribution of seasalt related aerosols was high (although the instrument is not designed to provide quantitative measurements of refractory material). In order to extract these seasalt related species and to avoid them dominating the organic aerosol spectra they were removed and classified into a seasalt related aerosol. This classification included ion signals at m/z 23 (Na⁺), m/z 58, m/z 60 (NaCl), m/z 81, m/z 83 (NaCl)Na⁺⁴⁵. Positive matrix factorization was then performed using the PMF evaluation tool v2.04. Organic related m/z (excluding those possibility linked with NaCl) from 0 to 200 amu were included in the analysis. The temporal variability in the organic signal was low, making it difficult to extract different sources of organic species.

Production fluxes calculations. The sea spray number flux F_{CN} (# m⁻² s⁻¹) was calculated from the SSA concentration (#m⁻³), flushing air flow (m³ s⁻¹) and surface of seawater in the sea spray generator (m²). F_{CN} can also be expressed as a function of the volume of air entrained in the seawater by the plunging jets system F_{ent} (m³ m⁻² s⁻¹) following Eq. (2):

$$F_{CN}(\# \text{ m}^{-2} \text{ s}^{-1}) = p F_{ent}(\text{m}^3 \text{ m}^{-2} \text{ s}^{-1}) \quad (2)$$

where p is the production efficiency per volume of air entrained, and F_{ent} the volume of air entrained. F_{ent} was measured as a function of seawater flow rate from our plunging jet system using an experimental setting that isolates a single jet from its environment equipped with an online air flowmeter, in a similar manner to that described by Salter et al. (2014)⁴⁶. For relating the fluxes obtained from the plunging jet system to a wind speed-related flux in the ambient atmosphere, we followed the approach from Long et al. (2011)⁴⁷. The authors calculate that the volume of air entrained in a plunging air system can be expressed as a function of wind speed at 10 m above sea level (Eq. 3)

$$F_{En} = 2 \times 10^{-8} U_{10}^{3.74} \quad (3)$$

Fluxes F_{CN} were calculated for the equivalent wind speed of each experiment, and then harmonized by using a U_{10} of 9 m s⁻¹ and 15 °C seawater temperature to compare fluxes between experiments. We normalized all fluxes to a given seawater temperature so as to isolate the biology impact-only on the SSA fluxes. The temperature dependence was calculated as given for inorganic sea salt by Salter et al. (2015)⁴⁸. This temperature correction induces an average 1.2% increase of the sea spray flux when the flux from Mediterranean seawaters (average 20.4 ± 1.2 °C) is calculated for 15 °C, and a negligible correction to the fluxes was found from arctic and NZ coastal waters (average 13.4 ± 1.9 °C and 17.7 ± 2.2 °C respectively). Using the same set-up as in the present study, Schwier et al. (2017)²⁴ measured an average total number flux of 3 × 10⁶ # m⁻² s⁻¹ for a SST of 22 °C in Mediterranean mesocosms seawaters. This would correspond in our parameterization to a nanophytoplankton cell abundance of 1130 cells ml⁻¹, which is in the range of nanophytoplankton cell abundances found for the PEACETIME voyage. Our inorganic total number flux are also consistent with number flux measurements from artificial seawater using similar experimental set-ups in Fuentes et al. 2010⁴¹ and Martensson et al. (2003)²⁶. We find a fairly good agreement with these two studies, despite the differences in SSA generation set ups, experimental conditions and flux calculation procedures. Both for the Fuentes (2010)⁴¹ and Martensson (2003)²⁶ parameterizations a flux of 9 × 10⁵ # m⁻² s⁻¹ is calculated for a wind speed of 9 m s⁻¹, compared to our inorganic number flux of 2.09 × 10⁵ # m⁻² s⁻¹. Finally, ambient air fluxes of 2 × 10⁶ m⁻² s⁻¹ for a wind speed of 9 m s⁻¹ were measured

in the Atlantic Ocean using the eddy correlation methods (Geever et al. 2005)⁴⁹, which would correspond to a nanophytoplankton cell abundance of 720 cells ml⁻¹ using our parameterization.

Seawater sampling and characterization. Seawater temperature and salinity were measured during PEACETIME using the onboard thermosalinometer. Chlorophyll-*a* was derived from the particulate absorption spectrum line-height at 676 nm⁵⁰, the relationship was adjusted to PEACETIME chlorophyll-*a* derived from HPLC ($\text{Chl-}a = 194.41 \times \text{line_height}^{1.131}$). POC was estimated from particulate attenuation at 660 nm using an empirical relationship specific to PEACETIME ($\text{POC} = 1405.1 \times c_p(660) - 52.4$) slightly higher than the literature which is likely due to the small dynamic range (1.27 higher on average for the range observed⁵¹). Both particulate attenuation and absorption of surface water were measured continuously with a WetLabs ACS using a flow-through system similar to the setup described in Slade et al. (2010)⁵². Phytoplankton cells were counted semi-continuously (one sample every hour) using an automated Cytosense flow cytometer (Cytobuoy, NL), connected to the continuous clean pumping system^{53,54}. The Cytosense pumped its sample from an isolated chamber of 200 ml filled in less than 30 s. Each sample was driven towards the flow cell by a calibrated peristaltic pump from which volume analyzed were calculated. Each particle in suspension in the sample was then separated one from the other through a laminar flow with a 0.1 μm filtered sea water sheath fluid, and crossed a laser beam (Coherent, 488 nm, 120 mV). The instrument recorded the pulse shapes emitted, resulting in: forward scatter (FWS) and sideward scatter (SWS) as well as red and orange fluorescences (FLR > 652 nm, FLO 552–652 nm respectively) in the size range < 1–800 μm in large and a few mm in length for chain forming cells. Laser scattering at small angles (FWS) was collected by two distinct photodiodes to check for the sample core alignment. Two trigger levels were applied for distinction between highly concentrated picophytoplankton and cyanobacteria groups (trigger level FLR 7.34 mV, sampling at a speed of 4 mm³ s⁻¹ analyzing 0.65 ± 0.18 cm³), and lower concentrated nano- and microphytoplankton (trigger level FLR 14.87 mV, at a speed of 8 mm³ s⁻¹ analyzing 3.57 ± 0.97 cm³). Different sets of 2D projections were plotted in Cytoclus software to manually gate phytoplankton groups. To ensure stability of the flow cytometer, 2 μm red fluorescing polystyrene beads (Polyscience) were regularly analyzed. The use of silica beads (1.0, 2.0 μm , 3.0 μm , 5.0 μm , 7.0 μm in diameter, Bangs Laboratory) for size retrieving estimates from FWS were used to separate picoplankton from nanoplankton clusters.

Arctic waters during MACA. During MACA, phytoplankton (< 20 μm) cell abundances were measured from a subsample of 1.6 mL collected daily for each mesocosm and fixed with glutaraldehyde following the protocol described in Marie et al. 2001⁵⁵, then stored at - 80 °C until analysis. The subsample was analysed with FacsCanto II cytometer (3-laser, 8-color (4–2–2), BD Biosciences) equipped with a 20 mW 488 nm coherent sapphire solid state blue laser to evaluate the abundance of cyanobacteria, pico (< 2 μm) and nanophytoplankton (2–20 μm), as described by Pecqueur et al. 2011⁵⁶. During ME3, NanoPhyto were measured by Flow Cytometry using techniques detailed in Safi and Hall (2001)⁵⁷.

Surface microlayer (SML) sampling and analysis. During PEACETIME, surface microlayer SML sampling was conducted from a zodiac using a 50 × 26 cm silicate glass plate sampler⁵⁸ with an effective sampling surface area of 2600 cm² considering both sides. For sampling, the zodiac was steered 0.5 nautical miles away from the research vessel and into the wind direction to avoid contamination. The glass plate was immersed perpendicular to the sea surface and withdrawn at ~ 17 cm s⁻¹. SML samples were removed from the plate using a Teflon wiper⁵⁵ and collected in an acid cleaned and rinsed bottle. Prior to sampling, all equipment was cleaned with acid (10% HCl) and rinsed in MilliQ and copiously rinsed with seawater directly before samples were taken.

The abundance and area of TEP were quantified by microscopy⁵⁹. Depending on the concentration of TEP, 40–50 ml of sample was filtered onto a 0.4 μm Nucleopore membrane (Whatman) and stained with 1 ml Alcian Blue solution (0.2 g l⁻¹ w/v) for 3 s. Filters were mounted on Cytoclear slides and stored at - 20 °C until analysis with a Zeiss Axio Scope.A1 (Zeiss). Images were taken with an AxioCam MRC (Zeiss) and analysed with ImageJ⁶⁰. Filters with MilliQ water served as a blank.

Ocean color satellite-based estimates of NanoPhyto cellular abundances. Monthly surface NanoPhyto cellular abundances were estimated. Essentially, the method of Uitz et al. (2006)³⁹ was applied to the surface chlorophyll *a* concentration derived from the MODIS entire mission monthly composites (9-km spatial resolution). The monthly mixed layer depth data required as input to the method was taken from the climatology of de Boyer Montégut et al. (2004)⁶¹. This procedure yields estimates of the contribution of nanophytoplankton (comprising nano-eukaryotes and coccolithophores) to total chlorophyll *a* biomass (in units of mg chlorophyll-*a* m⁻³) within the global ocean, except coastal waters and inland seas. These estimates were then converted into cellular abundances (in units of cells mL⁻¹) using an assumed intracellular chlorophyll content of 2.64 × 10⁻¹⁰ mg chlorophyll a cell⁻¹ for the NanoPhyto group. This was computed as the median of the intracellular chlorophyll content values given in Stramski et al. (2010)⁶² for phytoplankton species within the nanophytoplankton class.

Received: 29 July 2020; Accepted: 5 November 2020

Published online: 11 January 2021

References

1. Carslaw, K. *et al.* Large contribution of natural aerosols to uncertainty in indirect forcing. *Nature* **503**, 67–71 (2013).

2. Glassmeier, F. *et al.* An emulator approach to stratocumulus susceptibility. *Atmos. Chem. Phys.* **19**, 10191–10203, <https://doi.org/10.5194/acp-19-10191-2019> (2019).
3. Rosenfeld, D., Zhu, Y., Wang, M., Zheng, Y., Goren, T., Yu, S. Aerosol-driven droplet concentrations dominate coverage and water of oceanic low-level clouds. *Science* **363** (64276427) (2019).
4. Fossum, K.N., Ovadnevaite, J., Ceburnis, D., Dall'Osto, M., Marullo, S., Bellacicco, M., Simó, R., Liu, D., Flynn, M., Zuend, A., O'Dowd, C. Summertime primary and secondary contributions to southern ocean cloud condensation nuclei. *Sci. Rep.* **8**(11), 13844. <https://doi.org/10.1038/s41598-018-32047-4> (2018).
5. Chubb, T. *et al.* Observations of high droplet number concentrations in Southern Ocean boundary layer clouds. *Atmos. Chem. Phys.* **16**, 971–987, <https://doi.org/10.5194/acp-16-971-2016> (2016).
6. Meskhidze, N. & Nenes, A. Phytoplankton and cloudiness in the Southern Ocean. *Science* <https://doi.org/10.1126/science.1131779> (2006).
7. McCoy, D. T. *et al.* Natural aerosols explain seasonal and spatial patterns of Southern Ocean cloud albedo. *Sci. Adv.* <https://doi.org/10.1126/sciadv.1500157> (2015).
8. Quinn, P. K. & Bates, T. S. The case against climate regulation via oceanic phytoplankton sulphur emissions. *Nature* **480**, 51–56. <https://doi.org/10.1038/nature10580> (2011).
9. Ducklow, H. W. *et al.* Dissolved organic carbon as a component of the biological pump in the North Atlantic Ocean. *Philos. Trans. R. Soc. B* **348**(1324), 161–167 (1995).
10. O'Dowd, C. D. *et al.* A combined organic-inorganic sea-spray source function. *Geophys. Res. Lett.* **35**(1), L01801 (2008).
11. Sciare, J. *et al.* Long-term observations of carbonaceous aerosols in the Austral Ocean atmosphere: Evidence of a biogenic marine organic source. *J. Geophys. Res.* **114**(D15), D15302 (2009).
12. Rinaldi, M. *et al.* Is chlorophyll-a the best surrogate for organic matter enrichment in submicron primary marine aerosol?. *J. Geophys. Res. Atmos.* **118**, 4964–4973 (2013).
13. Schwier, A. N. *et al.* Primary marine aerosol emissions from the Mediterranean Sea during pre-bloom and oligotrophic conditions: Correlations to seawater chlorophyll-a from a mesocosm study. *Atmos. Chem. Phys.* **15**, 7961–7976, <https://doi.org/10.5194/acp-15-7961-2015>(2015).
14. Forestieri, S. D. *et al.* Temperature and composition dependence of sea spray aerosol production. *Geophys. Res. Lett.* <https://doi.org/10.1029/2018GL078193> (2018).
15. Fuentes, E., Coe, H., Green, D., de Leeuw, G. & McFiggans, G. On the impacts of phytoplankton-derived organic matter on the properties of the primary marine aerosol – Part 1: Source fluxes. *Atmos. Chem. Phys.* **10**, 9295–9317, <https://doi.org/10.5194/acp-10-9295-2010> (2010).
16. Alpert, P. A. *et al.* The influence of marine microbial activities on aerosol production: A laboratory mesocosm study. *J. Geophys. Res. Atmos.* **120**, 8841–8860 (2015).
17. Russell, L. M., Hawkins, L. N., Frossard, A. A., Quinn, P. K. & Bates, T. S. Carbohydrate-like composition submicron atmospheric particles and their production from ocean bubble bursting. *Proc. Natl. Acad. Sci. USA* **107**, 6652–6657. <https://doi.org/10.1073/pnas.0908905107> (2010).
18. Ovadnevaite, J. *et al.* Primary marine organic aerosol: A dichotomy of low hygroscopicity and high CCN activity. *Geophys. Res. Lett.* **38**, L21806. <https://doi.org/10.1029/2011GL048869> (2011).
19. Yoon, Y. J. *et al.* Seasonal characteristics of the physicochemical properties of North Atlantic marine atmospheric aerosols. *J. Geophys. Res.* **112**, 04206. <https://doi.org/10.1029/2005JD007044> (2007).
20. Long, M. S. *et al.* Light-enhanced primary marine aerosol production from biologically productive seawater. *Geophys. Res. Lett.* **41**, 2661–2670 (2014).
21. Westervelt, M. D., Moore, R. H., Nenes, A. & Adams, P. J. Effect of primary organic sea spray emissions on cloud condensation nuclei concentrations. *Atmos. Chem. Phys.* **12**, 89–101 (2012).
22. Gantt, B., Meskhidze, N. The physical and chemical characteristics of marine primary organic aerosol: A review. *Atmos. Chem. Phys.* **13**, 3979–3996, <https://doi.org/10.5194/acp-13-3979-2013> (2013).
23. Collins, D. B. *et al.* Phytoplankton blooms weakly influence the cloud forming ability of sea spray aerosol. *Geophys. Res. Lett.* **43**, 9975–9983. <https://doi.org/10.1002/2016GL069922> (2016).
24. Schwier, A. N. *et al.* Primary marine aerosol physical and chemical emissions during a nutrient enrichment experiment in mesocosms of the Mediterranean Sea. *Atmos. Chem. Phys.* **17**, 14645–14660, <https://doi.org/10.5194/acp-17-14645-2017>(2017).
25. Freney, E., Sellegri, K., Nicosia, A., Trueblood, J., Rinaldi, M., Williams, L.R., Prévôt, A. S. H., Thyssen, M., Grégori, G., Haëntjens, N., Dinasquet, J., Obernosterer, I., Van-Wambeke, F., Engel, A., Zäncker, B., Desboeuf, K., Asmi, E., Guieu, C. Mediterranean nascent sea spray organic aerosol and relationships with seawater biogeochemistry.
26. Martensson, E. M., Nilsson, E. D., de Leeuw, G., Cohen, L. H., Hansson, H.-C. Laboratory simulations and parameterization of the primary marine aerosol production. *J. Geophys. Res.-Atmos.* **108**, 4297, <https://doi.org/10.1029/2002JD002263> (2003).
27. Salter, M. E., Zieger, P., Acosta Navarro, J. C., Grythe, H., Kirkevåg, A., Rosati, B., Riipinen, I., Nilsson, E. D. An empirically derived inorganic sea spray source function incorporating sea surface temperature. *Atmos. Chem. Phys.* **15**, 11047–11066, <https://doi.org/10.5194/acp-15-11047-2015> (2015).
28. Paterson, M. P. & Spillane, K. T. Surface films and the production of sea-salt aerosol. *Q. J. R. Meteorol. Soc.* **95**, 526–534 (1969).
29. Van Vleet, E. S. & Williams, P. M. Surface potential and film pressure measurements in seawater systems. *Limnol. Oceanogr.* **28**, 401–414 (1983).
30. Zábory, J., Matisāns, M., Krejci, R., Nilsson, E. D. & Ström, J. Artificial primary marine aerosol production: A laboratory study with varying water temperature, salinity, and succinic acid concentration. *Atmos. Chem. Phys.* **12**, 10709–10724, <https://doi.org/10.5194/acp-12-10709-2012> (2012).
31. Modini, R. L., Russell, L. M., Deane, G. B. & Stokes, M. D. Effect of soluble surfactant on bubble persistence and bubble-produced aerosol particles. *J. Geophys. Res.* **118**, 1388–1400. <https://doi.org/10.1002/jgrd.50186> (2013).
32. Tyree, C. A., Hellion, V. M., Alexandrova, O. A. & Allen, J. O. Foam droplets generated from natural and artificial seawaters. *J. Geophys. Res.* **112**, D12204. <https://doi.org/10.1029/2006JD007729> (2007).
33. Garrett, W. D. Influence of monomolecular surface films on production of condensation nuclei from bubbled sea water. *J. Geophys. Res.* **73**, 5145–5150. <https://doi.org/10.1029/JB073i016p05145> (1968).
34. Alldredge, A. L., Passow, U. & Logan, B. E. The abundance and significance of a class of large, transparent organic particles in the ocean. *Deep-Sea Res. Pt I*(40), 1131–1140. [https://doi.org/10.1016/0967-0637\(93\)90129-Q](https://doi.org/10.1016/0967-0637(93)90129-Q) (1993).
35. Facchini, M. C., Rinaldi, M., Decesari, S., Carbone, C., Finessi, E., Mircea, M., Fuzzi, S., Ceburnis, D., Flanagan, R., Nilsson, E.D., de Leeuw, G., Martino, M., Woeltjen, J., O'Dowd, C.D. Primary submicron marine aerosol dominated by insoluble organic colloids and aggregates. *Geophys. Res. Lett.* **35**, 17814, <https://doi.org/10.1029/2008GL034210> (2008).
36. O'Dowd, C. D. *et al.* Connecting marine productivity to sea-spray via nanoscale biological processes: Phytoplankton dance or death disco?. *Sci. Rep.* **5**(1), 14883. <https://doi.org/10.1038/srep14883> (2015).
37. Trainic, M. *et al.* Infection dynamics of a bloom-forming alga and its virus determine airborne coccolith emission from seawater. *Science* **6**, 327–335. <https://doi.org/10.1016/j.isci.2018.07.017> (2018).
38. Uitz, J., Claustre, H., Morel, A. & Hooker, S. B. Vertical distribution of phytoplankton communities in open ocean: An assessment based on surface chlorophyll. *J. Geophys. Res.* **111**, C08005. <https://doi.org/10.1029/2005JC003207> (2006).

39. Burrows, S. M., Easter, R., Liu, X., Ma, P.-L., Wang, H., Elliott, S. M., Singh, B., Zhang, K., Rasch, P. J. OCEANFILMS sea-spray organic aerosol emissions—Part 1: Implementation and impacts on clouds. *Atmos. Chem. Phys. Discuss.* (in review), <https://doi.org/10.5194/acp-2018-70> (2018).
40. Sellegri, K., Odowd, C. D., Yoon, Y. J., Jennings, S. G., Deleeuw, G. Surfactants and submicron sea spray generation. *J. Geophys. Res.* <https://doi.org/10.1029/2005JD006658> (2006)
41. Fuentes, E., Coe, H., Green, D., de Leeuw, G. & McFiggans, G. Laboratory-generated primary marine aerosol via bubble-bursting and atomization. *Atmos. Meas. Tech.* **3**, 141–162, <https://doi.org/10.5194/amt-3-141-2010> (2010).
42. Asmi, E. *et al.* Aerosol cloud activation in summer and winter at puy-de-Dôme high altitude site in France. *Atmos. Chem. Phys.* **12**, 11589–11607, <https://doi.org/10.5194/acp-12-11589-2012> (2012).
43. Ng, N. *et al.* Real-time methods for estimating organic component mass concentrations from aerosol mass spectrometer data. *Environ. Sci. Technol.* **45**, 910–916. <https://doi.org/10.1021/es102951k> (2011).
44. Allan, J. D. *et al.* A generalised method for the extraction of chemically resolved mass spectra from Aerodyne aerosol mass spectrometer data. *J. Aerosol Sci.* **35**, 909–922 (2004).
45. Schmale, J. *et al.* Sub-Antarctic marine aerosol: Dominant contributions from biogenic sources. *Atmos. Chem. Phys.* **13**, 8669–8694 (2013).
46. Salter, M. E., Nilsson, E. D., Butcher, A. & Bilde, M. On the seawater temperature dependence of continuous plunging jet derived sea spray aerosol. *J. Geophys. Res.* **119**, 9052–9072. <https://doi.org/10.1002/2013JD021376> (2014).
47. Long, M. S., Keene, W. C., Kieber, D. J., Erickson, D. J. & Maring, H. A sea-state based source function for size- and composition-resolved marine aerosol production. *Atmos. Chem. Phys.* **11**, 1203–1216 (2011).
48. Salter, M. E. *et al.* An empirically derived inorganic sea spray source function incorporating sea surface temperature. *Atmos. Chem. Phys.* **15**, 11047–11066 (2015).
49. Geever, M., O'Dowd, C., van Ekeren, S., Flanagan, R., Nilsson, D., de Leeuw, G., Rannik, U. Sub-micron sea-spray fluxes. *Geophys. Res. Lett.* **32**, 15810. <https://doi.org/10.1029/2005GL023081> (2005).
50. Boss, E., Picheral, M., Leeuw, T., Chase, A., Karsenti, E., Gorsky, G., Taylor, L., Slade, W., Ras, J., Claustre, H. The characteristics of particulate absorption, scattering and attenuation coefficients in the surface ocean; Contribution of the Tara Oceans expedition. *Methods Oceanogr.* (2013).
51. Cetinic, I., Perry, M. J., Briggs, N. T., Kallin, E., D'Asaro, E. A., Lee, C. M. Particulate organic carbon and inherent optical properties during 2008 North Atlantic bloom experiment. *J. Geophys. Res. Oceans.* <https://doi.org/10.1029/2011JC007771> (2012)
52. Slade, W. H. *et al.* Underway and moored methods for improving accuracy in measurement of spectral particulate absorption and attenuation. *J. Atmos. Ocean. Technol.* **27**(10), 1733–1746 (2010).
53. Thyssen, M. *et al.* Onset of the spring bloom in the northwestern Mediterranean Sea: Influence of environmental pulse events on the in situ hourly-scale dynamics of the phytoplankton community structure. *Front. Microbiol.* **5**, 387. <https://doi.org/10.3389/fmicb.2014.00387.2014> (2010).
54. Leroux, R. *et al.* Combining laser diffraction, flow cytometry and optical microscopy to characterize a nanophytoplankton bloom in the northwestern Mediterranean. *Progr. Oceanogr.* **163**, 248–259. <https://doi.org/10.1016/j.pocean.2017.10.010> (2017).
55. Marie, D., Partensky, F., Vaulot, D., & Brussaard, C. Enumeration of phytoplankton, bacteria, and viruses in marine samples. in *Current Protocols in Cytometry*. (Wiley, 2001). <https://doi.org/10.1002/0471142956.cy1111s10>.
56. Pecqueur, D. *et al.* Dynamics of microbial planktonic food webcomponents during a river flash flood in a Mediterranean coastal lagoon. *Hydrobiologia* **673**, 13–27 (2011).
57. Hall, J. A. & Safi, K. The impact of in situ Fe fertilisation on the microbial food web in the Southern Ocean. *Deep Sea Res. Part II* **48**, 2591–2613. [https://doi.org/10.1016/S0967-0645\(01\)00010-8](https://doi.org/10.1016/S0967-0645(01)00010-8) (2001).
58. Cunliffe, M. & Wurl, O. *Guide to Best Practices to Study the Ocean's Surface* (Occasional Publications of the Marine Biological Association of the United Kingdom, Plymouth, 2014).
59. A. Engel, Determination of marine gel particles. in *Practical Guidelines for the Analysis of Seawater* (eds Oliver W., ed.), 125–142 (CRC Press Taylor & Francis Group, Boca Raton) (2009).
60. Schneider, C. A., Rasband, W. S. & Eliceiri, K. W. NIH Image to Image: 25 years of image analysis. *Nat. Methods* **9**, 671–675. <https://doi.org/10.1038/nmeth.2089> (2012).
61. de Boyer Montégut, C., Madec, G., Fischer, A. S., Lazar, A., Iudicone, D. Mixed layer depth over the global ocean: An examination of profile data and a profile-based climatology. *J. Geophys. Res.* **109**, C12003, <https://doi.org/10.1029/2004JC002378>. (2004).
62. Stramski, D., Bricaud, A. & Morel, A. Modeling the inherent optical properties of the ocean based on the detailed composition of the planktonic community. *Appl. Opt.* **40**, 2929–2945. <https://doi.org/10.1364/AO.40.002929> (2001).

Acknowledgements

We thank Lisa Northcote for sample collection, Karen Thompson for Flow Cytometry analysis, Karl Safi for optical microscopy, and Neill Barr and Mark Gall for assistance with the NZ Coastal mesocosm experiment. The underway optical instrumentation was provided by Emmanuel Boss's group funded by Nasa Ocean Biology and Biogeochemistry. The authors would like to thank Christophe Salmeron and David Pecqueur from the UPMC/CNRS cytometry/imaging platform of the Banyuls Oceanographic Observatory for MACA microbial phytoplankton analysis.

Author contributions

K.S. conceptualized the emission studies within Peacetime, MACA and CARIM projects. K.S., A.N., E.F., J.U., M.P. and J.T. contributed to formal analysis of the aerosol data and J.U., M.T., G.G., A.E., B.Z., N.H., S.M., A.S.-M., D.L. contributed to formal analysis of the seawater data. K.S., C.G., K.D., B.D. and C.L. contributed to funding acquisition of the Peacetime, MACA/PARCS and ME3 projects. K.S., A.N., M.T., G.G., A.E., B.Z., N.H., S.M., D.P., A.S.-M., C.R., D.L. and C.L. contributed to investigation. K.S., C.G., K.D., C.L. contributed to project administration. K.S., C.G., M.T. and C.L. wrote the original draft. All authors contributed to writing and revision of the work.

Funding

This study is a contribution to the PEACETIME project (<http://peacetime-project.org>) (<https://doi.org/10.17600/17000300>), a joint initiative of the MERMEX and ChArMEX components supported by CNRS-INSU, IFREMER, CEA, and Météo-France as part of the program MISTRALS coordinated by INSU. Within PEACETIME, Bio-optical measurements were performed within the project CNES PEACETIME-OC. PEACETIME was endorsed as a process study by GEOTRACES. The Arctic mesocosm experiment was carried out in the frame of the MACA (Marine Aerosol impact on Clouds in the Arctic) project financed by IPEV, and PARCS (Pollution in the ARctic

System) financed by INSU. The NZ mesocosm experiment (ME3) was supported by NZ MBIE funding for the CARIM (Coastal Acidification: Rate, Impacts & Management) Project. This work has also received funding from the ANR T-ERC Sea2Cloud and from the European Research Council (ERC) under the European Union's Horizon 2020 research and innovation program (Sea2Cloud grant agreement No 771369). Sea2Cloud was endorsed by SOLAS. The Peacetime POC determination was funded by the French Space Agency (CNES) through the COYOTE project (CNES/TOSCA program) led by Hubert Loisel and Lucile Duforêt-Gaurier.

Competing interests

The authors declare no competing interests.

Additional information

Supplementary information is available for this paper at <https://doi.org/10.1038/s41598-020-78097-5>.

Correspondence and requests for materials should be addressed to K.S.

Reprints and permissions information is available at www.nature.com/reprints.

Publisher's note Springer Nature remains neutral with regard to jurisdictional claims in published maps and institutional affiliations.



Open Access This article is licensed under a Creative Commons Attribution 4.0 International License, which permits use, sharing, adaptation, distribution and reproduction in any medium or format, as long as you give appropriate credit to the original author(s) and the source, provide a link to the Creative Commons licence, and indicate if changes were made. The images or other third party material in this article are included in the article's Creative Commons licence, unless indicated otherwise in a credit line to the material. If material is not included in the article's Creative Commons licence and your intended use is not permitted by statutory regulation or exceeds the permitted use, you will need to obtain permission directly from the copyright holder. To view a copy of this licence, visit <http://creativecommons.org/licenses/by/4.0/>.

© The Author(s) 2021